

LA-UR-21-30444

Accepted Manuscript

Laser spot welding of additive manufactured 304L stainless steel

Hawk, Cheryl Lynn
Simonds, Brian
Tanner, Jack
Pacheco, Robin Montoya
Brand, Michael J.
Vigil, Greg
Javernick, Daniel Anthony
Liu, Stephen

Provided by the author(s) and the Los Alamos National Laboratory (2022-05-10).

To be published in: Welding in the World

DOI to publisher's version: 10.1007/s40194-022-01265-w

Permalink to record:

<http://permalink.lanl.gov/object/view?what=info:lanl-repo/lareport/LA-UR-21-30444>



Los Alamos National Laboratory, an affirmative action/equal opportunity employer, is operated by Triad National Security, LLC for the National Nuclear Security Administration of U.S. Department of Energy under contract 89233218CNA000001. By approving this article, the publisher recognizes that the U.S. Government retains nonexclusive, royalty-free license to publish or reproduce the published form of this contribution, or to allow others to do so, for U.S. Government purposes. Los Alamos National Laboratory requests that the publisher identify this article as work performed under the auspices of the U.S. Department of Energy. Los Alamos National Laboratory strongly supports academic freedom and a researcher's right to publish; as an institution, however, the Laboratory does not endorse the viewpoint of a publication or guarantee its technical correctness.

Laser Spot Welding of Additive Manufactured 304L Stainless Steel

Cheryl Hawk^{1,3}, Brian Simonds^{1,2}, Jack Tanner², Robin Pacheco³,
Michael Brand³, Greg Vigil¹, Daniel Javernick³, and Stephen Liu¹

1-Colorado School of Mines, 2-National Institute of Standards and Technology - Boulder, CO,
3-Los Alamos National Laboratory

Abstract

The goal of this work is to understand if an additively manufactured 304L stainless steel exhibits similar spot-welding behavior as wrought 304L stainless steel. Due to the many differences between an additively manufactured component and wrought product, it is important to determine how the material interacts with the laser and how it affects the weld bead morphology. In this paper, the laser coupling efficiency, weld size, and solidification of spot welds produced in wrought and additively manufactured 304L stainless steel were investigated. The coupling efficiency of wrought and additively manufactured 304L stainless steel of similar surface condition were approximately the same over a range of applied laser energies. Laser welding of the untreated (rougher) surface of additively manufactured 304L, however, showed improved coupling efficiency ranging between 3.3% and 100%. The rougher surface traps the incoming light and increases the coupling efficiency at lower laser energies, while at higher energy, the absorption efficiency is dominated by intrinsic absorption from the keyhole formation rather than surface roughness. The resulting spot weld microstructures differed from welds made in wrought 304L and additively manufactured 304L. Welds made in wrought 304L were fully austenitic containing what is suspected to be massive austenite, which suggests that these welds solidified as primary ferrite. Welds made in additively manufactured 304L were also fully austenitic and contained both cellular austenite and what is suspected to be massive austenite. These observations mean that welds made in additively manufactured 304L solidified as primary ferrite and primary austenite. The differences in weld microstructures made in wrought and AM 304L can be attributed to differences in the composition and solidification rate.

Introduction

Additive manufacturing (AM) has sparked much interest for industrial applications due to the ability to create one-of-a-kind, complex components in a relatively rapid manner. Though there are many possibilities to implement an additively manufactured component, the applications are limited because the weldability of such components has not been thoroughly studied. Therefore, additively manufactured components are not typically applied to regions that require a joint. As expected, build volumes are limited by the chamber size. To implement larger AM components, welding or joining methods would be required to implement larger scale AM components. For this reason, it is important to understand the welding behavior of an additive manufactured component and determine if it behaves similar to a wrought or cast component.

There are many factors from the AM process that are of concern for the welding and joining quality of these AM components. First, powder AM components are known to have less minor element control than wrought or cast products [1-5]. Typically, in stainless steelmaking the material is refined using an argon oxygen decarburization (AOD) furnace and/or a vacuum

oxygen decarburization (VOD) furnace to remove impurities [6]. Minor elements, such as oxygen and nitrogen, can be introduced back into the stainless steel during the powder atomization processes [3-5, 6]. Oxygen, a surface-active element, affects the surface tension gradient and therefore the molten metal flow in the weld pool [7]. This phenomenon is known as Marangoni flow [7-9]. He et al. determined that fluid flow in laser spot welds is mainly surface tension driven, which suggests that there might be a difference in spot weld morphology between welds made in AM and wrought 304L, if there is a difference in oxygen content [10]. Nitrogen is an austenite-stabilizing element that, in excess, hinders primary ferrite solidification, decreases the amount of delta ferrite in the microstructure, and limits the deformation induced martensitic transformation [2, 3, 11].

Second, AM components experience a complex thermal history, similar to but not the same as multipass welding. Due to the rapid heating and cooling results from the AM scan strategy, a significant amount of residual stress can develop within AM components [12-14]. Residual stresses within the component can lead to part distortion [15-18] and defects such as cracking [19]. It is possible that welding over a component with high residual stresses could relieve some of the stresses, but it could also result in reheat cracking near the heat affected zone (HAZ) [20-22].

Third, AM components can possibly contain defects. Both the type and number of defects represent issues for autogenous laser welding of an AM component. With a large number of defects, underfill during autogenous welding becomes an issue where a concavity is left in the weldment, which may form a centerline crack. If the laser were to scan over gas entrapment, the expelled gas could interfere with the vapor plume, thus resulting in weld instability and different weld characteristics. These three concerns are some of the major reasons why the weldability of AM material should be researched.

This research focuses on the laser-material interaction of spot welds produced in wrought 304L and AM 304L. It is important to understand if AM material absorbs laser energy the same as wrought material. If each material absorbs different amounts of energy, welding differences could result. Laser coupling efficiency was calculated from the measured dynamic absorptivity using an integrating sphere in order to quantify the differences between wrought and AM 304L.

Experimental Procedure

AM Build Parameters

Laser powder bed fusion builds were created at Los Alamos National Laboratory (LANL) using an EOS M280 powder bed system¹. Virgin powder manufactured by argon gas atomization was used for this build. The powder contained a spherical morphology with average particle size of 31 μm [23]. The builds were produced with dimensions of 50.8 mm x 38.1 mm x 3 mm (2 in. x 1.5 in. x 0.12 in.) as shown in Figure 1. The core of the builds was created with a laser power of 195 W, a travel speed of 1000 mm/s, and a beam offset of 0.015 mm. Once the core of the build is completed, the laser scans around the perimeter of the part, known as the contour of the build. The first contour, made closest to the core, was made with a laser power of 140 W, a travel speed of 1400 mm/s, and a beam offset of 0.012 mm. The second contour was created with a

laser power of 80 W, a travel speed of 800 mm/s, and no beam offset. The beam offset is a defined distance set inwards from the edge geometry. The powder layer thickness was 40 μm and the scan strategy rotated 67° with every layer. The builds produced with these parameters were fully dense and fully austenitic. The microstructure of the AM builds is shown in Figure 2.

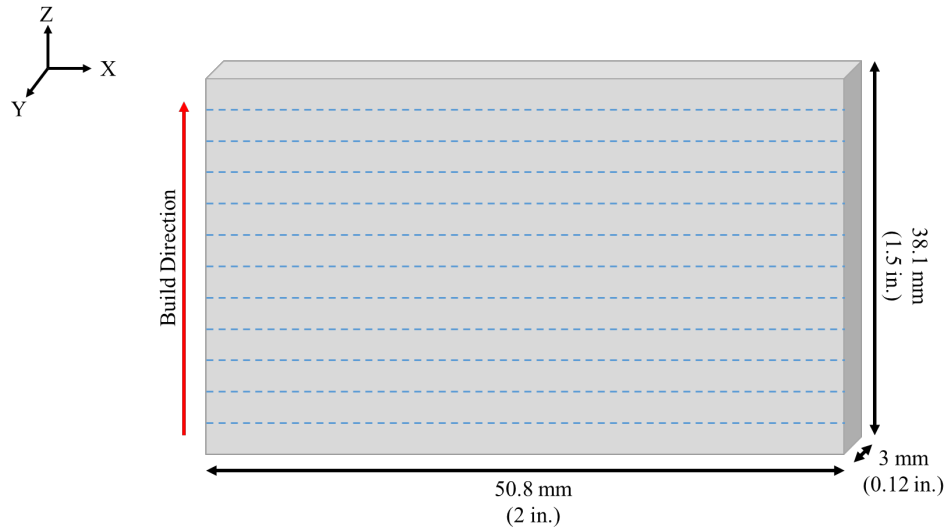


Figure 1: Schematic of the laser powder bed fusion build dimensions with dashed lines indicating the boundaries of the layers.

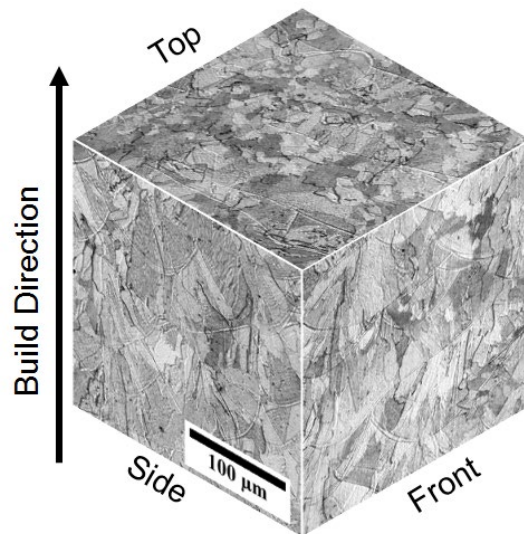


Figure 2: Representative microstructure of AM build.

¹Certain commercial equipment, instruments, or materials are identified in this paper in order to specify the experimental procedure adequately. Such identification is not intended to imply recommendation or endorsement by NIST, nor is it intended to imply that the materials or equipment identified are necessarily the best available for the purpose.

Material Preparation

Absorptance is affected by temperature, surface roughness, physical and electrical properties of a material [24-30]. Polished metallic surfaces have lower absorptance due to the reflective surface [31, 32]. In general, absorptance of metals can be increased by increasing temperature and modifying the surface roughness [33]. Boyden and Zhang [26] determined that the absorptivity of AISI 304 stainless steel is higher than that of pure iron, suggesting that composition has an effect on laser absorptance. Therefore, different materials and surface roughness were studied.

Wrought 304L stainless steel was selected as a baseline comparison for the AM 304L samples. Wrought 17-4 material was also included in the study for comparison because it is a martensitic grade stainless steel with a larger difference in composition and microstructure. Most of the samples were studied in the as-received or as-built conditions, however, AM builds in the as-built condition are known to have significant amounts of residual stress [34]. In fact, when grinding the surface of the builds, the edges would start to curl indicating the presence of residual stress. Therefore, one AM sample underwent a stress-relief heat treatment at 1065°C for 30 min following specification AMS2759/4C [35]. Most of the samples were ground using 600 grit SiC paper resulting in an average surface roughness of about 7.5 μm . To determine the effect of surface finish, one of the as-built AM 304L samples was left untreated resulting in a surface roughness of about 30.5 μm . A summary of the various sample conditions is shown in Table 1 and the compositions are shown in Table 2.

Table 1: Material conditions used in experiment.

Material	Condition	Surface Finish	Comparisons
Wrought 17-4	As-received (AR)	Ground (GR) Sa = 7.57 μm	Martensitic, lower residual stress
Wrought 304L	As-received (AR)	Ground (GR) Sa = 7.08 μm	Austenitic, lower residual stress
AM 304L	As-built (AB)	Ground (GR) Sa = 7.49 μm	Austenitic, higher residual stress
AM 304L	As-built (AB)	Untreated (UT) Sa = 30.47 μm	Austenitic, higher residual stress, rough
AM 304L	Heat Treated (HT) 1065°C, 30 min	Ground (GR) Sa = 7.79 μm	Austenitic, lower residual stress

All the samples were cut into 12.7 mm x 12.7 mm x 3 mm (0.5 in x 0.5 in x 0.12 in) coupons. In the case of AM materials, the location of the coupon cut with respect to the build direction was recorded. After the coupon surfaces were prepared, they were cleaned using ethanol. The surfaces were analyzed using a commercial optical profilometer before and after spot welding. The spot weld diameters from the profilometry images were measured using image analysis software. The spot welds were then cross-sectioned, ground, and polished using standard metallographic techniques. Next, the samples were polished to 0.02 μm roughness using

colloidal silica on a commercial vibratory polisher for 4 hrs. Lastly, electro-etching was used with a solution containing 50% nitric acid and 50% deionized water which revealed the solidification substructure. The weld width and weld depths were measured from the etched cross-sections.

Table 2: Composition of 304L Powder, AM 304L (as-built and heat treated), wrought 304L, and wrought 17-4 stainless steels in weight percent (with balance of iron).

Material	C	Cr	Cu	Mn	Mo	N	Ni	O	P	S	Si	Cr _{req} /Ni _{req}
Powder 304L	0.011	18.41	-	1.52	0.004	0.053	9.56	0.038	0.005	0.002	0.58	1.67
AB, AM 304L	0.012	18.48	0.011	1.42	-	0.049	9.85	0.051	-	0.004	0.51	
HT, AM 304L	0.013	18.02	0.011	1.37	-	0.050	9.55	0.071	-	0.004	0.51	
Wrought 304L	0.043	18.22	-	0.90	-	0.049	8.06	0.006	0.037	0.004	0.40	1.73
Wrought 17-4	0.050	15.90	3.20	0.50	-	-	4.00	-	-	0.0002	0.30	-

Laser Spot Welding

Laser welding absorptivity experiments were conducted at the National Institute of Standards and Technology (NIST) in Boulder, CO and followed a similar procedure and experimental set up as the experiments conducted by Simonds et al. [36, 37]. The experiments used an integrating sphere which allowed the user to measure the scattered light and calculate the absorptance and resulting coupling efficiency of the various materials. A gas port was added to the integrating sphere to shield the molten pool during welding. The sphere was purged with nitrogen shielding gas for 2 min and left flowing during the welding process at a rate of 18 L/min. This experiment was limited to spot welding as the accuracy is dependent upon the calibration of the integrating sphere. After each spot weld, some of the vapor is deposited onto the inner surface of the sphere, thus reducing the effectiveness of the coating. This changing surface condition is why the sphere must be calibrated after each spot weld. Long time duration, linear welds would cause vapor deposition along the walls of the integrating sphere resulting in degradation of the effectiveness of the coating and the calibration would change as a function of time. A commercial Yb-fiber laser system with a 1070 nm wavelength was used to produce 10 ms spot welds. The laser operated under sharp focus, producing a spot size of 303 μm and a top-hat beam profile.

Results and Discussion

Laser Coupling Efficiency

The time-integrated laser coupling efficiency as a function of the applied laser energy for wrought 304L stainless steel is shown in Figure 3. As the applied laser energy increases, the coupling efficiency also increases, albeit with smaller increases for higher applied laser energies.

Others have similarly observed a step-function relationship for the coupling efficiency of 316L stainless steel [36, 38, 39]. The sharp increase in coupling efficiency, between the two dashed lines, has been identified as the transition region. At the lower applied laser energy, conduction mode welding takes place. The spot weld labeled 1.18 J show a wide, shallow weld that is indicative of conduction mode. The dashed line on the left marks the beginning of the transition region, meaning that sufficient vaporization has occurred to begin the formation of a keyhole. At such a low energy, the vapor cavity is not stable and surface tension forces the cavity to close. Within this region, deeper penetration should begin to form, but because the vapor cavity is unstable, the penetration depth is relatively small. The micrograph labeled 2.55 J exhibits the spot weld produced at the beginning of the transition region. The arrow within this micrograph shows a deepening at the root of the spot weld that indicates penetration depth is starting to increase more than would typically occur under conduction mode. As the input laser energy increases to 3.55 J and 4.56 J, the depression becomes more pronounced and the depth of penetration becomes larger confirming that keyhole mode has been established as shown in the micrograph labeled 4.56 J.

Figure 4(a) demonstrates the laser coupling efficiencies for spot welds produced in wrought 304L, AM 304L, and wrought 17-4 stainless steels prepared with the same ground (GR) surface finish. The coupling efficiency values are shown in Table A-1 of the appendix. Within the combined measurement of uncertainty (coupling efficiency error bars represent a coverage factor of 1), there is no discernable difference in laser coupling efficiency between the three different stainless steels. This suggests that composition and microstructural effects on coupling efficiency of various stainless steels are negligible. The results observed by Boyden and Zhang [26] were between pure iron and 304L. Since negligible differences were observed between 304L and 17-4, the coupling efficiency is affected by large compositional changes and not minor changes, i.e. pure material with respect to an alloy.

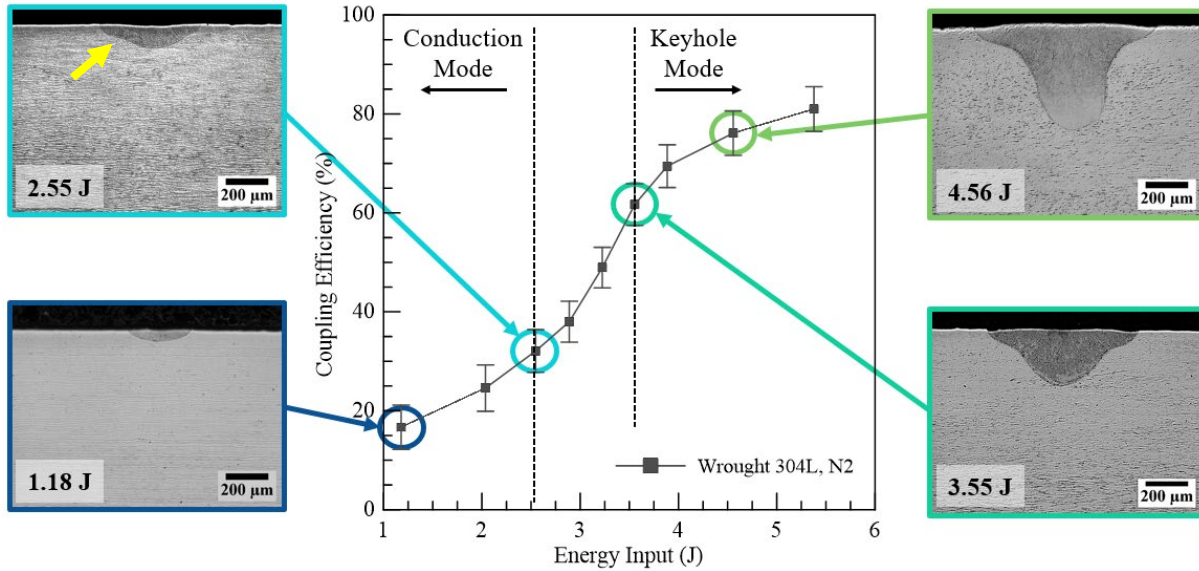


Figure 3: Coupling efficiency for spot welds produced in wrought 304L stainless steel with corresponding cross-sectioned micrographs.

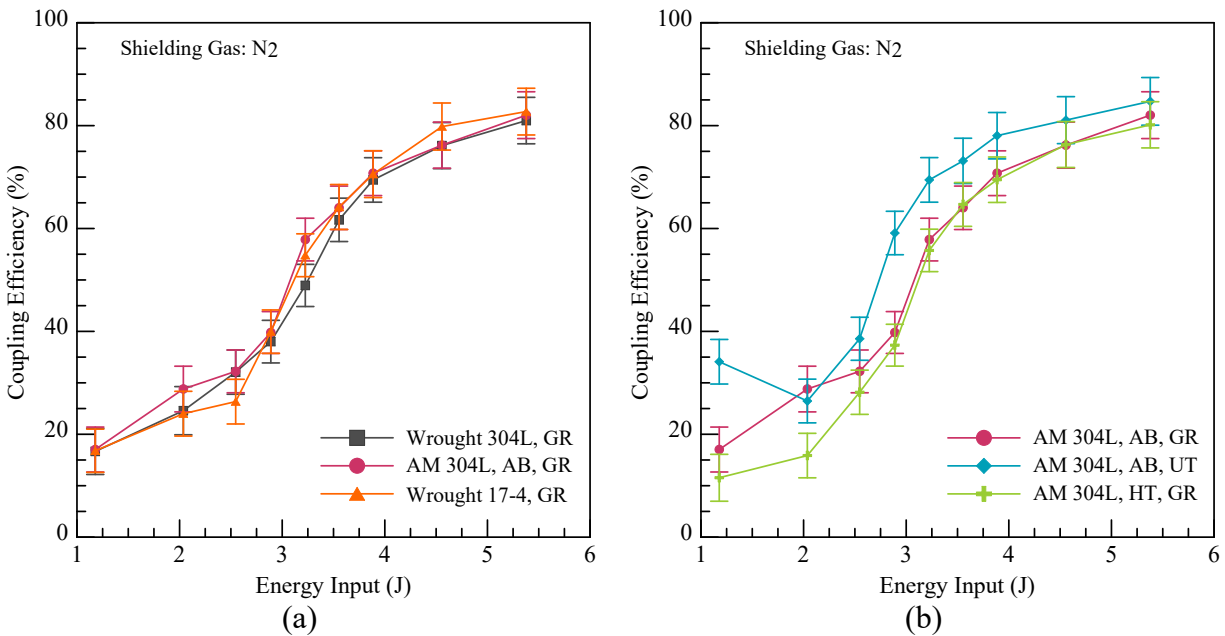


Figure 4: Laser coupling efficiency for spot welds produced in (a) wrought 304L, AM 304L, and wrought 17-4 stainless steels prepared with the same surface finish and (b) AM 304L stainless steels under the various conditions.

Figure 4(b) shows the laser coupling efficiencies for spot welds produced in AM 304L under the different conditions named in Table 1, namely, heat treatment and surface finish. The corresponding coupling efficiency values are shown in Table 3. Welds produced in the AM 304L samples prepared with the same, ground, surface finish have similar laser coupling efficiencies. The largest difference in behavior occurs for the spot welds produced in the untreated (UT) condition (designated by the blue diamonds). The untreated condition, with a larger surface

roughness, resulted in increased coupling efficiencies compared to the ground conditions. A rough surface allows for increased surface scattering at the larger peaks and troughs, leading to an improved initial coupling efficiency. This observation is consistent with the results of Sokolov and Salminen [33]. The effect of surface roughness is larger at lower applied laser energies than at higher applied laser energies. At lower applied laser energies, the coupling efficiency is improved by 20% - 100%, however, at higher applied laser energies the coupling efficiency is improved by only 3% - 20%. When keyhole mode is established, the multiple reflections experienced in the cavity that forms by the vapor plume dominates absorption as the laser is no longer incident to a solid surface. The ground, heat treated condition (designated by the green cross) is about the same as the ground, as-built condition (designated by the pink circles). Since heat treatment would have relieved any residual stresses in the weld coupon prior to welding, the observed behavior means that residual stress and starting microstructure have a negligible effect on the coupling efficiency.

Table 3: Coupling efficiency for spot welds made in AM 304L in the as-built (AB), ground (GR) condition, as-built (AB), untreated (UT) condition, and the heat treated (HT), ground (GR) condition. The uncertainty in the data is 1 sigma.

Applied Laser Power (W)	Applied Laser Energy (J)	AM 304L AB GR ($\eta_{\text{coupling, \%}}$)	AM 304L AB UT ($\eta_{\text{coupling, \%}}$)	AM 304L HT GR ($\eta_{\text{coupling, \%}}$)
118	1.18	17.0 ± 4.4	34.1 ± 4.3	11.6 ± 4.6
204	2.04	28.8 ± 4.4	26.5 ± 4.2	15.9 ± 4.3
255	2.55	32.2 ± 4.2	38.6 ± 4.2	28.2 ± 4.3
289	2.89	39.8 ± 4.1	59.1 ± 4.2	37.3 ± 4.1
323	3.23	57.9 ± 4.2	69.5 ± 4.3	55.7 ± 4.1
356	3.55	64.0 ± 4.2	73.2 ± 4.4	64.7 ± 4.3
389	3.89	70.8 ± 4.4	78.0 ± 4.5	69.5 ± 4.4
456	4.56	76.2 ± 4.5	81.1 ± 4.6	76.3 ± 4.5
538	5.38	82.0 ± 4.6	84.7 ± 4.6	80.2 ± 4.5

Spot Weld Morphology

Macrographs of the spot welds produced with increasing energies ranging between 1.18 J and 4.56 J in the austenitic grade stainless steels (wrought and AM 304L) are shown in Figure 5. The corresponding weld width and depth measurements are shown in Figure 6, with the values listed in Table A-2 of the appendix. At the lowest applied laser energy of 1.18 J, the spot welds produced on a ground surface were wide and shallow, which is typical of conduction mode welds. The weld width of the spot weld produced in wrought 304L is slightly wider than welds produced in AM 304L by about 8.5 %, demonstrated in Figure 6(a). The depth of penetration of the spot weld produced in wrought 304L at 1.178 J is shallower than spot welds produced in AM 304L by 21.8 %. These data may indicate that the lower surface-active element concentration in wrought 304L is the cause for the difference in weld morphology. The differences between wrought and AM 304L at 1.18 J is not as obvious as the results from Kou et al. [9]. The smaller differences could be due to the limited weld duration of this experiment or due to oxygen being

the major surface-active element rather than sulfur, due to the fact that oxygen has less of an impact on Marangoni flow compared to sulfur.

At lower applied laser energies, the untreated surface of the AM 304L samples have resulted in deeper penetration. This is attributed to lower specular reflections from the rougher surface compared to the ground surface resulting in surface scattering thus improving the coupling efficiency at lower laser energies. This correlates well with the measured coupling efficiency results for both types of surfaces. At higher applied laser energies, the depth of penetration is about the same for samples prepared in the untreated condition and ground condition, thus, agreeing with the earlier supposition that surface roughness is less relevant after keyhole formation where multiple reflections dominate.

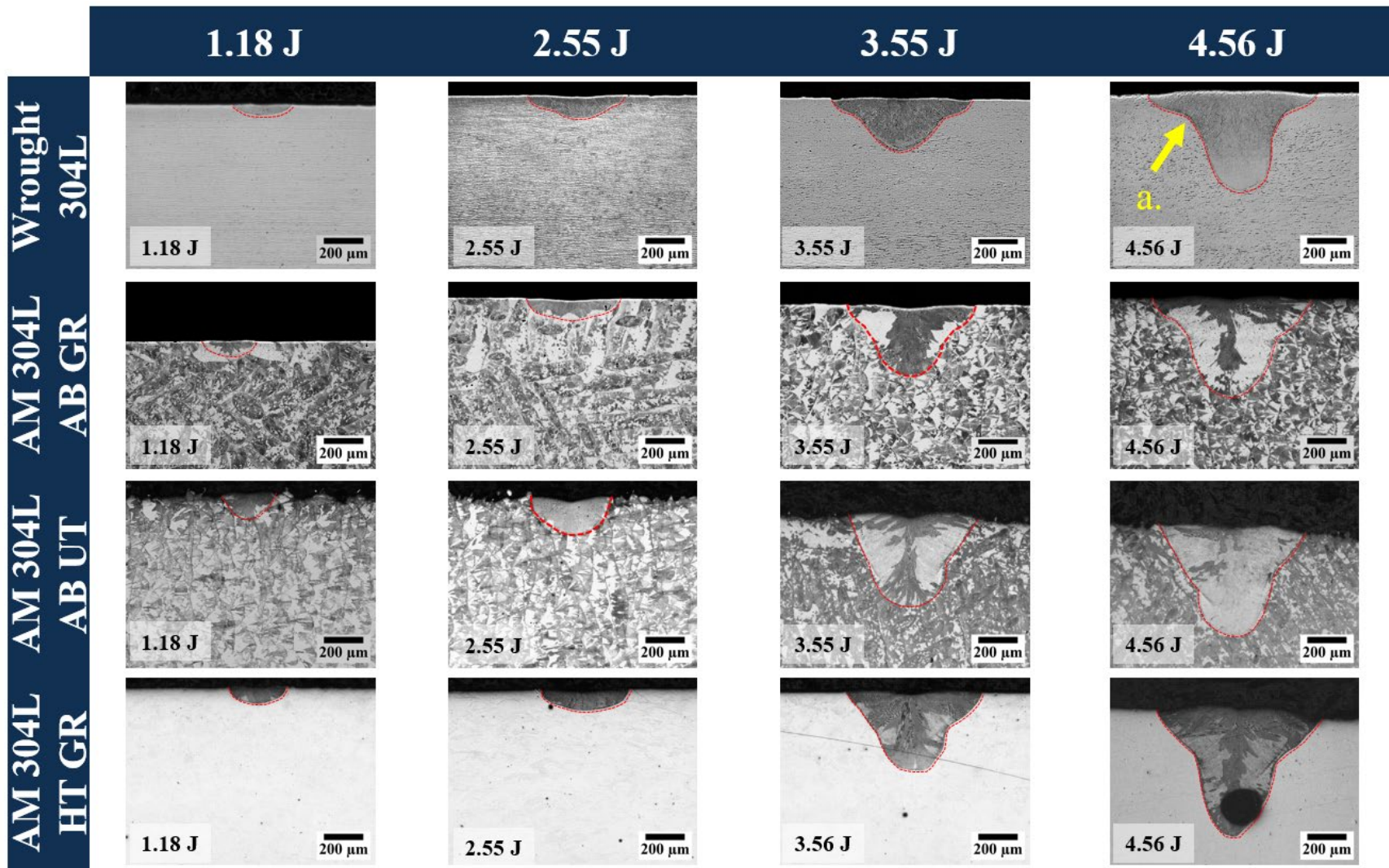


Figure 5: Representative macrographs of spot welds produced in wrought 304L and the various conditions of additive manufactured 304L stainless steels. The fusion lines are outlined by the red dashed lines.

Welds produced in AM 304L produced at 2.55 J, beginning of the transition region, have a rounder fusion line morphology. Whereas the spot weld produced in wrought 304L shows a deepening of the root that was discussed earlier in Figure 3. Deepening of the root becomes more pronounced with increasing applied laser energies for most of the spot welds. The location and nature of the pronounced root is different for spot welds produced in the untreated AM 304L samples. It is possible that the rougher surface affects the laser-material interaction enough to change the morphology slightly.

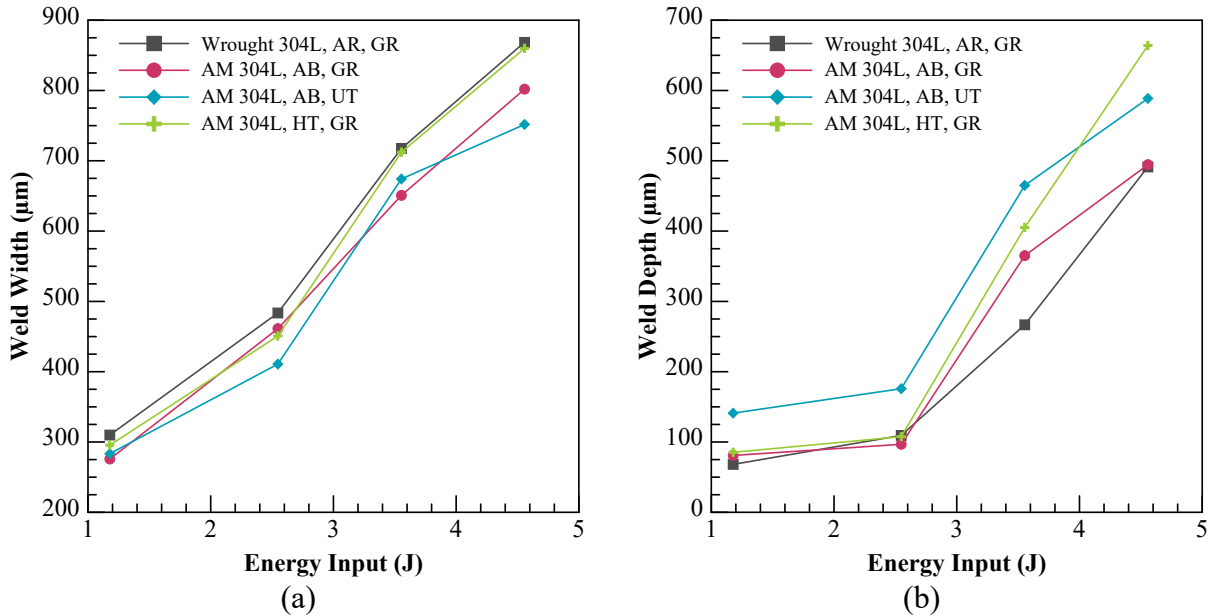


Figure 6: (a) Weld width and (b) weld depth measurements of spot welds produced in the various 304L stainless steel conditions.

As the applied laser energy increases, the depth of penetration and weld width increases as shown in Figure 6. At higher laser energies, differences in weld bead morphology between the various samples become more apparent. The increased heat input causes more stirring, and the recoil force dominates over surface tension. These might be the reason why differences in morphology become larger. In general, the welds produced in wrought 304L are wider and shallower than welds produced in AM 304L. A larger number of repetitions of spot welds would better confirm the trend.

Spot Weld Microstructure

A representative macrograph and micrograph of a spot weld produced in wrought 304L with a laser input energy of 3.55 J is shown in Figure 7. The cross-section in Figure 7(a) suggests a superposition of two heat flow conditions – a semi-hemisphere (red dotted trace) which is an indication of conduction heat transfer and a central region of deeper penetration (blue dotted trace) which is evidence of keyhole mode. The microstructure, shown in Figure 7(b), contains a fully austenitic microstructure. Some of the grains within the weldment are ill-defined,

characteristic of a massive transformation [40, 41]; however, not all the grains suspected to be massive austenite exhibit the ill-defined grains as observed previously [42]. There are small black spots seen in the microstructure also observed by Wilson [42] in massive austenite grains. The ill-defined grain boundaries, small black spots, and fully austenitic microstructure is an indication that the spot weld solidified as primary ferrite and then underwent a massive austenite transformation known as type F/MA solidification. This type of solidification behavior occurred for all the spot welds produced in wrought 304L stainless steel. Almost all of the spot welds exhibited solidification cracking as shown by the arrow in Figure 7(b). Solidification cracking most likely occurred due to the large concentration of phosphorous in the base material. Phosphorous concentrations above 0.025 wt. % are known to cause hot cracking, despite solidification as primary ferrite [43]. Changing the applied laser energy did not change the resulting spot weld microstructure and all spot welds contained a massive austenite microstructure.

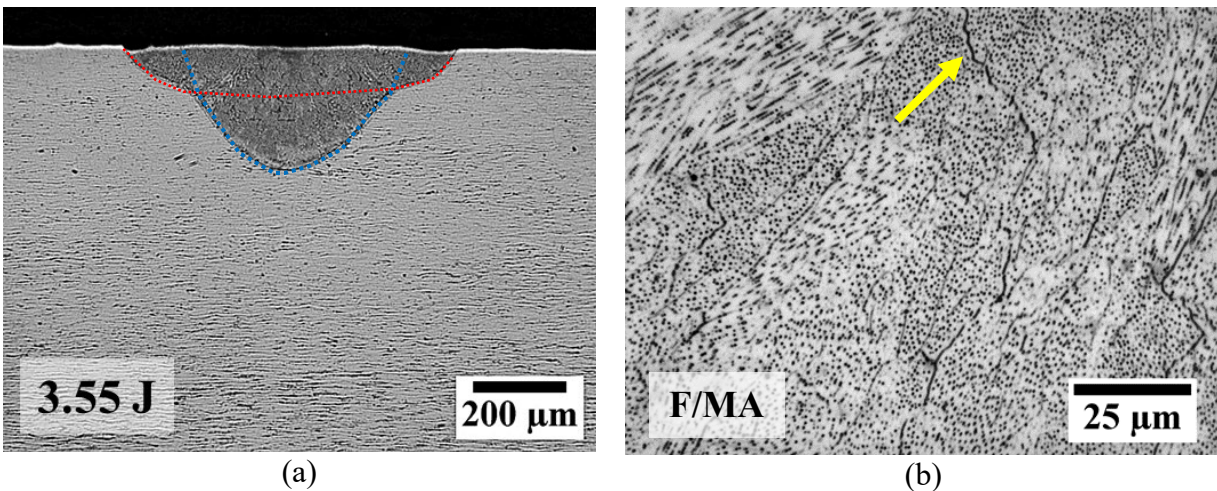


Figure 7: Representative (a) macrograph and (b) micrograph of a spot weld produced in wrought 304L at a laser input energy of 3.55 J. The arrow points to cracking that occurred during solidification.

A representative macrograph and micrograph of a spot weld produced in as-built AM 304L with the ground surface finish is shown in Figure 8. The macrograph shown in Figure 8(a) shows a marked difference in etching behavior compared to the spot weld made in wrought 304L (Figure 7). The micrograph in Figure 8(b) shows a completely austenitic microstructure. The solidification substructure changes from the edge of the weld to the center of the weld. At the weld edge (left half of the micrograph), within the lighter colored regions, the weld solidified as primary ferrite that underwent a massive austenite transformation. The lighter region exhibits no clear evidence of substructure, only irregular grains and similar black spots as seen in Figure 7(b). As the solid/liquid interface approached the weld center, the solidification mode shifted to primary austenite, forming a cellular austenite substructure known as Type A solidification. This

change suggests that the solidification rate or composition has changed during solidification to cause a shift in the solidification mode and type of solidification substructure. It is well established that solidification rate changes from the edge of a weld to the center of the weld. By increasing the input laser energy, there was a decrease in the amount of primary austenite solidification, thus reducing the amount of cellular substructure as demonstrated in Figure 9, with values available in Appendix A-3. Increasing the laser input energy results in increasing heat input and decreasing the solidification rate producing more type F/MA solidification.

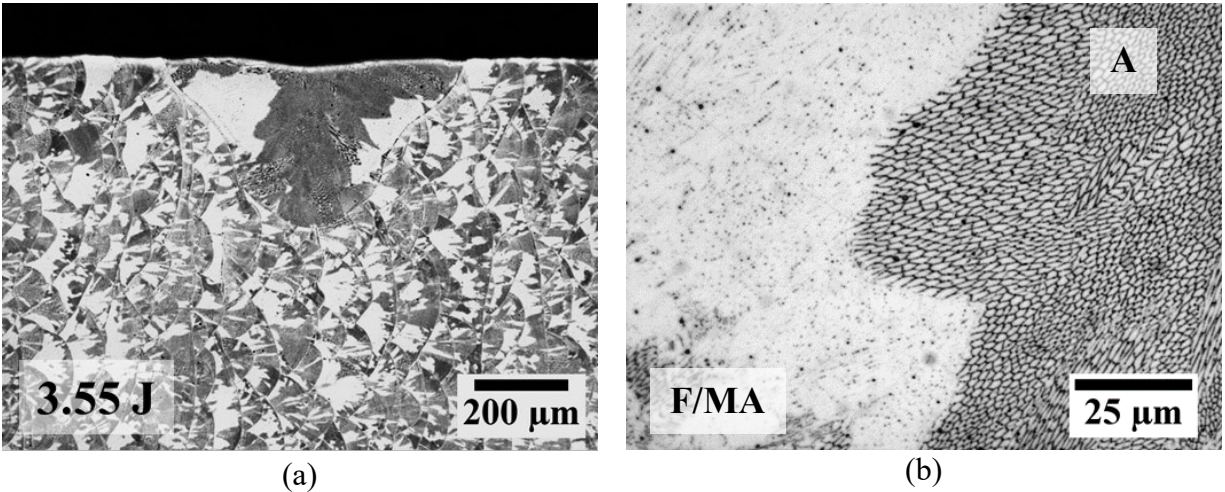


Figure 8: Representative (a) macrograph and (b) micrograph of a spot weld produced in as-built AM 304L with a ground surface at a laser input energy of 3.55 J.

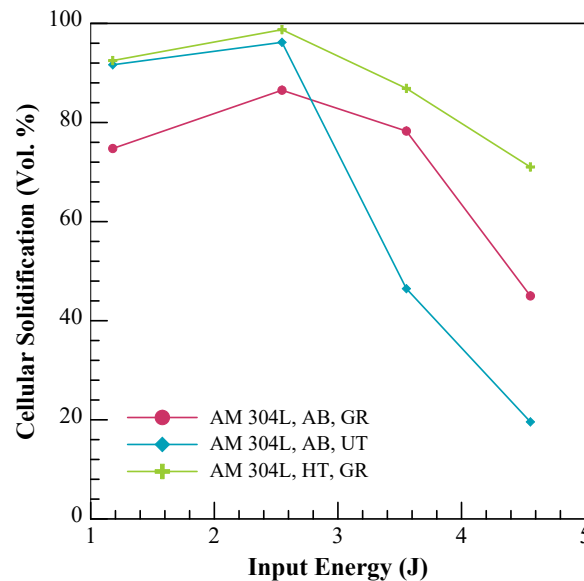


Figure 9: Volume percent of cellular austenite solidification substructure observed in the spot welds produced in additive manufactured 304L under the various conditions.

Measurement of the solidification rate for laser spot welds is challenging because traditional measurements cannot be used due to the lack of travel speed. An estimate of solidification rate can be made by plotting the Cr_{eq}/Ni_{eq} in the stainless steel predictive diagram which was modified from Lippold and Kotecki [44], shown in Figure 10. A dashed line was placed to indicate a range of solidification rates that were possible given the spot weld microstructures. The blue dashed line for AM 304L demonstrates that for the AM 304L composition, the solidification behavior may change from F/MA to A given an increase in solidification rate (moving up along the blue dashed line). Zhao et al. [45] determined that the solidification rate increases as the solidification front approaches the weld center for spot welds made in Ti-6Al-4V. This observation could explain why there was a shift from primary ferrite solidification to primary austenite solidification for the spot weld made in AM 304L. The red dashed line for wrought 304L shows that even with an increase in solidification rate, the solidification should remain as primary ferrite in the F/MA domain. These results indicate that compositional differences between wrought and AM 304L have a very large impact on the solidification behavior.

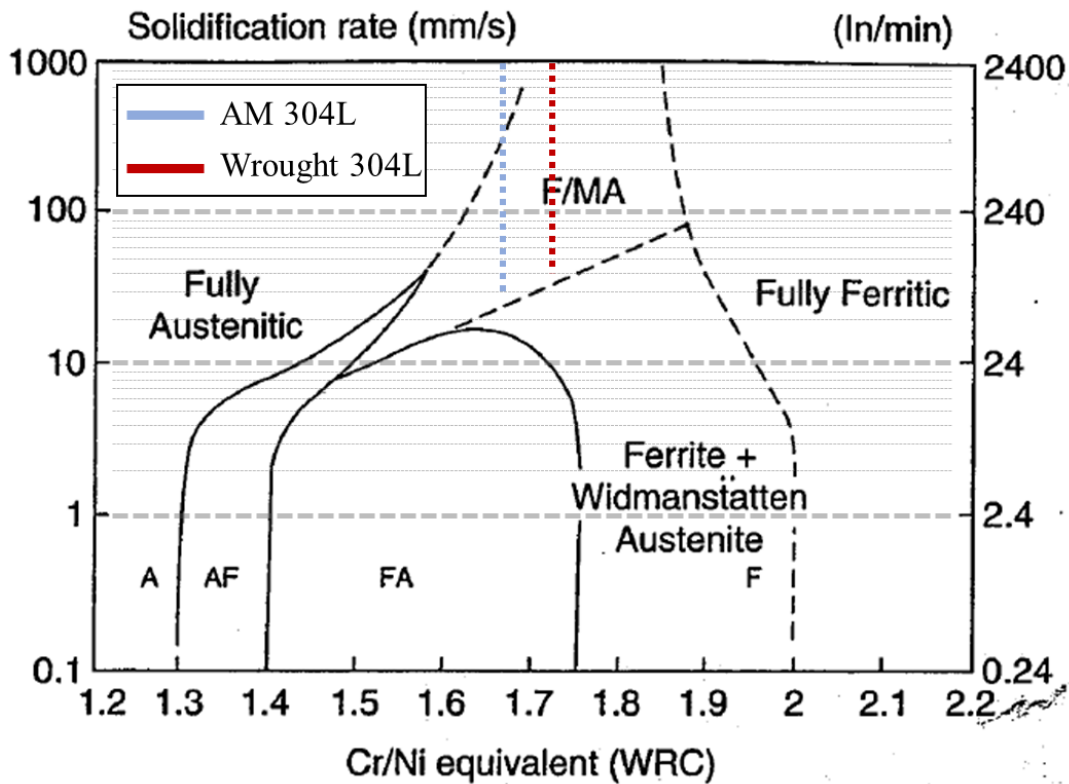


Figure 10: A morphological prediction map for stainless steels modified to contain the Cr_{eq}/Ni_{eq} for Wrought 304L and AM 304L. Adapted from Lippold and Kotecki [44]

Conclusions

There are two variables identified from the laser powder bed fusion process that affected the welding and solidification behavior of AM 304L stainless steel compared to wrought 304L stainless steel: the surface condition and starting composition. The major conclusions are listed in the following:

- (1) The laser powder bed process produces a rougher surface finish than a ground surface. As a result, the as-built, untreated surface produced higher coupling efficiencies at lower energies that is attributed to multiple reflections established at earlier times. The increased coupling efficiency produced spot welds with deeper penetration.
- (2) Laser coupling efficiency was not affected by composition or starting microstructure. Wrought 17-4, a martensitic stainless steel, showed similar laser coupling efficiency as the austenitic stainless steels.
- (3) Spot welds produced in wrought 304L stainless steel resulted in fully austenitic microstructure that solidified as primary ferrite and underwent a massive transformation to austenite (Type F/MA). The higher Cr_{eq}/Ni_{eq} as compared with AM 304L, stabilized the primary ferrite solidification so that an increase in solidification rate would not change the solidification mode. The shift in solidification mode is caused by the lower Cr_{eq}/Ni_{eq} for AM 304L and the increasing solidification rate as the solidification front approaches the weld center.
- (4) Spot welds produced in AM 304L stainless steel resulted in a fully austenitic microstructure that exhibited both primary ferrite and primary austenite solidification. Grains that solidified as primary ferrite subsequently underwent a massive transformation to austenite (Type F/MA solidification). As the solidification front approached the weld center, the solidification mode changed to primary austenite resulting in a cellular substructure (Type A solidification).

Appendix

Further data to supplement the discussion presented in this work. The data in these tables were used in the plotting of Figures 2, 3, 4 and 5. They help to support the discussion on increases in coupling efficiency described in the figures. The data also supports the weld width and weld penetration discussion summarized in Figures 4 and 5.

Table A-1: Coupling efficiency for spot welds made in wrought 304L, AM 304L, and wrought 17-4 with the same ground surface finish. The uncertainty in the data is 1 sigma.

Applied Laser Power (W)	Applied Laser Energy (J)	Wrought 304L AR GR (η_{coupling})	AM 304L AB GR (η_{coupling})	Wrought 17-4 AR GR (η_{coupling})
118	1.18	16.7 ± 4.5	17.0 ± 4.4	16.8 ± 4.2
204	2.04	24.6 ± 4.7	28.8 ± 4.4	24.0 ± 4.3
255	2.55	32.1 ± 4.3	32.2 ± 4.2	26.4 ± 4.3
289	2.89	38.0 ± 4.1	39.5 ± 4.0	40.0 ± 4.2
323	3.23	48.9 ± 4.1	57.9 ± 4.2	54.8 ± 4.2
355	3.55	61.7 ± 4.2	64.0 ± 4.2	64.2 ± 4.4
389	3.89	69.4 ± 4.3	70.8 ± 4.4	70.6 ± 4.6
456	4.56	76.1 ± 4.5	76.2 ± 4.5	79.8 ± 4.6
538	5.38	81.0 ± 4.5	82.0 ± 4.6	82.7 ± 4.5

Table A-2: Weld depth and weld width values for welds produced in the various conditions.

Material	Applied Laser Energy (J)	Weld Depth (μm)	Weld Width (μm)
Wrought 304L AR, GR	1.18	68.2	310.0
	2.55	109.0	483.0
	3.55	267.0	717.0
	4.56	491.0	868.0
AM 304L AB, GR	1.18	80.9	276.0
	2.55	96.7	461.0
	3.55	365.0	651.0
AM 304L AB, UT	4.56	494.0	802.0
	1.18	141.0	283.0
	2.55	176.0	411.0
AM 304L HT, GR	3.55	465.0	674.0
	4.56	589.0	752.0
	1.18	85.3	296.0
AM 304L HT, GR	2.55	108.0	451.0
	3.55	405.0	712.0
	4.56	664.0	860.0

Table A-3: Substructure volume fraction for welds produced in additive manufactured 304L.

Material	Applied Laser Energy (J)	Cellular %	Dendritic %
AM 304L AB, GR	1.18	74.8	25.2
	2.55	86.5	13.5
	3.55	78.3	21.7
	4.56	45.0	55.0
AM 304L AB, UT	1.18	91.7	8.4
	2.55	96.2	3.8
	3.55	46.5	53.5
	4.56	19.6	80.4
AM 304L HT, GR	1.18	92.5	7.5
	2.55	98.7	1.3
	3.55	86.9	13.1
	4.56	71.0	29.0

References

- [1] D. Gu and Y. Shen, “Balling phenomena in direct laser sintering of stainless steel powder: metallurgical mechanisms and control methods,” *Materials & Design*, vol. 30, no. 8, pp. 2903-2910, Sept. 2009. DOI: <https://doi.org/10.1016/j.matdes.2009.01.013>
- [2] S. Cheruvathur, E. A. Lass, and C. E. Campbell, “Additive manufacturing of 17-4 PH stainless steel: post-processing heat treatment to achieve uniform reproducible microstructure,” *JOM*, vol. 68, no. 3, pp. 930-942, Mar. 2016. DOI: <https://doi.org/10.1007/s11837-015-1754-4>
- [3] S. D. Meredith, J. S. Zuback, J. S. Keist, T. A. Palmer, “Impact of composition on the heat treatment response of additively manufactured 17-4 PH grade stainless steel,” *Materials Science & Engineering A*, vol. 738, pp. 44-56, Dec. 2016. DOI: <https://doi.org/10.1016/j.msea.2018.09.066>
- [4] M. Z. Gao, B. Ludwig, and T. A. Palmer, “Impact of atomization gas on characteristics of austenitic stainless steel powder feedstocks for additive manufacturing,” *Powder Technology*, 2020. DOI: <https://doi.org/10.1016/j.powtec.2020.12.005>
- [5] J. H. Park and H. Todoroki, “Control of MgO·Al₂O₃ spinel inclusions in stainless steels,” *Iron and Steel Institute of Japan International*, vol. 50, no. 10, pp. 1333-1346, 2010.
- [6] S. Naboychenko and N. A. Yefimov, *Handbook of Non-Ferrous Metal Powders: Technology and Application*, O. Neikov, Ed., Oxford: Elsevier, 2018.
- [7] C. R. Heiple, J. R. Roper, R. T. Stagner, and R. J. Aden, “Surface active element effects on the shape of GTA, laser, and electron beam welds,” *Welding Journal*, vol. 62, no. 3, pp.72-77, Mar. 1983.

- [8] J. R. Roper, "Mechanism for minor element effect on GTA fusion zone geometry," *Welding Journal*, vol. 61, no. 4, pp. 97-102, Apr. 1982.
- [9] S. Kou, C. Limmaneevichitr, and P. S. Wei, "Oscillatory Marangoni flow laser welding: a fundamental study by conduction-mode laser spot welding," *Welding Journal*, vol. 90, no. 12, pp. 229-240, Dec. 2011.
- [10] X. He, P. W. Fuerschbach, and T. Debroy, "Heat transfer and fluid flow during laser spot welding of 304L stainless steel," *Journal of Physics D: Applied Physics*, vol. 36, no. 12, pp. 1388-1398, May 2003.
- [11] U. K. Viswanathan, S. Banerjee, and R. Krishnan, "Effects of aging on the microstructure of 17-4 PH stainless steel," *Material Science and Engineering A*, vol. 104, pp. 181-189, Oct. 1988. DOI: [https://doi.org/10.1016/0025-5416\(88\)90420-X](https://doi.org/10.1016/0025-5416(88)90420-X)
- [12] C. Li, Z. Y. Liu, X. Y. Fang, and Y. B. Guo, "Residual stress in metal additive manufacturing," *Procedia CIRP*, vol. 71, pp. 348-353, Jan. 2018. DOI: <https://doi.org/10.1016/j.procir.2018.05.039>
- [13] M. Shiomi, K. Osakada, K. Nakamura, T. Yamashita, and F. Abe, "Residual stress within metallic model made by selective laser melting process," *CIRP Annals*, vol. 53, no. 1, pp. 195-198, Jan. 2004. DOI: [https://doi.org/10.1016/S0007-8506\(07\)60677-5](https://doi.org/10.1016/S0007-8506(07)60677-5)
- [14] P. Mercelis and J. Kruth, "Residual stresses in selective laser sintering and selective laser melting," *Rapid Prototyping Journal*, vol. 12, no. 5, pp. 254-265, Oct. 2006. DOI: <https://doi.org/10.1108/13552540610707013>
- [15] P. A. Colegrove *et al.*, "Microstructure and residual stress improvement in wire and arc additively manufactured parts through high-pressure rolling," *Journal of Materials Processing Technology*, vol. 213, no. 10, pp. 1782-1791, Oct. 2013. DOI: <https://doi.org/10.1016/j.jmatprotec.2013.04.012>
- [16] J. Ding *et al.*, "Thermo-mechanical analysis of wire and arc additive layer manufacturing process on large multi-layer parts," *Computer Material Science*, vol. 50, no. 12, pp. 3315-3322, Dec. 2011. DOI: <https://doi.org/10.1016/j.commatsci.2011.06.023>
- [17] N. Keller and V. Ploshikhin, "New method for fast predictions of residual stress and distortion of AM parts," *Solid Freeform Fabrication Symposium*, vol. 25, pp. 1229-1237, Aug. 2014.
- [18] B. A. Szost *et al.*, "A comparative study of additive manufacturing techniques: Residual stress and microstructural analysis of CLAD and WAAM printed Ti-6Al-4V components," *Materials & Design*, vol. 89, pp. 559-567, Jan. 2016. DOI: <https://doi.org/10.1016/j.matdes.2015.09.115>
- [19] X. Gong, T. Anderson, and K. Chou, "Review on powder-based electron beam additive manufacturing technology," *Manufacturing Review*, vol. 1, pp. 1-12, Mar. 2014. DOI: <https://doi.org/10.1051/mfreview/2014001>

- [20] A. Dhooge and A. Vinckier, "Reheat cracking – a review of recent studies," *International Journal of Pressure Vessels and Piping*, vol. 27, no. 4, pp. 239-269, Sept. 1987. DOI: [https://doi.org/10.1016/0308-0161\(87\)90012-3](https://doi.org/10.1016/0308-0161(87)90012-3)
- [21] Q. Auzoux, L. Allais, C. Caës, I. Monnet, A. F. Gourgues, and A. Pineau, "Effect of pre-strain on creep of three AISI 316 austenitic stainless steels in relation to reheat cracking of weld-affected zones," *Journal of Nuclear Materials*, vol. 400, no. 2, pp. 127-137, May 2010. DOI: <https://doi.org/10.1016/j.jnucmat.2010.02.021>
- [22] P. J. Bouchard, P. J. Withers, S. A. McDonald, and R. K. Heenan, "Quantification of creep cavitation damage around a crack in a stainless steel pressure vessel," *Acta Materialia*, vol. 52, no. 1, pp. 23-34, Jan. 2004. DOI: <https://doi.org/10.1016/j.actamat.2003.08.022>
- [23] R. Pacheco, "Comparing powder characterization, mechanical properties, and microstructures of virgin and highly recycled 304L for the EOS M280", LANL, Los Alamos, NM, USA, June 2017. LA-UR 17-24483
- [24] A. P. Tadamalle, Y. P. Reddy, E. Ramjee, and V. Reddy, "Evaluation of Nd:YAG laser welding efficiencies for 304L stainless steel," *Procedia Materials Science*, vol. 6, pp. 1731-1739, Sept. 2014. DOI: <https://doi.org/10.1016/j.mspro.2014.07.160>
- [25] G. S. Arnold, "Absorptivity of several metals at 10.6 μm : Empirical expressions for the temperature dependence computed from Drude Theory," *Journal of Applied Optics*, vol. 23, no. 9, pp. 1434-1436, 1984. DOI: <https://doi.org/10.1364/AO.23.001434>
- [26] S. B. Boyden and Y. Zhang, "Temperature and wavelength-dependent spectral absorptivities of metallic materials in the infrared," *Journal of Thermophysics and Heat Transfer*, vol. 20, no. 1, pp. 9-15, 2006. DOI: <https://doi.org/10.2514/1.15518>
- [27] H. E. Bennett, J. M. Bennett, E. J. Ashley, and R. J. Motyka, "Verification of the anomalous-skin-effect theory for silver in the infrared," *Physical Review*, vol. 165, no. 3, pp. 755-764, Jan. 1968. DOI: <https://doi.org/10.1103/PhysRev.165.755>
- [28] T. J. Wieting and J. L. Derosa, "Effects of surface condition on the infrared absorptivity of 304 stainless steel," *Journal of Applied Physics*, vol. 50, no. 2, pp. 1071-1078, Feb. 1978. DOI: <https://doi.org/10.1063/1.326083>
- [29] J. T. Wang, C. I. Weng, J. G. Chang, and C. C. Hwang, "The influence of temperature and surface conditions on surface absorptivity in laser surface treatment," *J. appl. Phys.*, vol. 87, no. 7, pp. 3245-3253, Apr. 2000. DOI: <https://doi.org/10.1063/1.372331>
- [30] L. K. Ang, Y. Y. Lau, R. M. Gilgenbach, and H. L. Spindler, "Analysis of laser absorption on a rough metal surface," *Applied Physics Letters*, vol. 70, no. 6, pp. 696-698, Feb. 1997. DOI: <https://doi.org/10.1063/1.118242>

- [31] N. Boutalbi, M. N. Bouaziz, and M. Allouche, "Influence of temperature-dependent absorptivity on solid surface heated by CO₂ and Nd:YAG lasers," *Journal of Laser Applications*, vol. 28, no. 3, pp. 1-8, Aug. 2016. DOI: <https://doi.org/10.2351/1.4947311>
- [32] A. K. Nath, R. Sridhar, P. Ganesh, and R. Kaul, "Laser power coupling efficiency in conduction and keyhole welding of austenitic stainless steel," *Sādhanā*, vol. 27, no. 3, pp. 383-392, Jun. 2002.
- [33] M. Sokolov and A. Salminen, "Improving laser beam welding efficiency," *Engineering*, vol. 6, no. 9, pp. 559-571, 2014. DOI: <https://dx.doi.org/10.4236/eng.2014.69057>
- [34] A. S. Wu, D. W. Brown, M. Kumar, G. Gallegos, and W. E. King, "An experimental investigation into additive manufacturing induced residual stresses in 316L stainless steel," *Metallurgical and Materials Transactions A*, vol. 45A, pp. 6260-6270, Dec. 2014. DOI: <https://doi.org/10.1007/s11661-014-2549-x>
- [35] Heat treatment austenitic corrosion-resistant steel parts, AMS2759/4D, 2018.
- [36] B. J. Simonds, *et al.*, "Time-resolved absorptance and melt pool dynamics during intense laser irradiation of a metal," *Physical Review Applied*, vol. 10, no. 1, pp. 1-14, Oct. 2018. DOI: <https://doi.org/10.1103/PhysRevApplied.10.044061>
- [37] B. J. Simonds, E. J. Garboczi, T. A. Palmer, and P. A. Williams, "Dynamic laser absorptance measured in a geometrically characterized stainless-steel powder layer," *Physical Review Applied*, vol. 13, no. 2, pp. 1-15, Feb. 2020. DOI: <https://doi.org/10.1103/PhysRevApplied.13.024057>
- [38] T. R. Allen, W. Huang, J. R. Tanner, W. Tan, J. M. Fraser, and B. J. Simonds, "Energy-coupling mechanisms revealed through simultaneous keyhole depth and absorptance measurements during laser-metal processing," *Physical Review Applied*, vol. 13, no. 6, pp. 1-13, Jun. 2020. <https://doi.org/10.1103/PhysRevApplied.13.064070>
- [39] T. R. Allen, B. J. Simonds, J. R. Tanner, and J. M. Fraser, "Simultaneous *in operando* monitoring of keyhole depth and absorptance in laser processing of AISI 316 stainless steel at 200 kHz," *Procedia CIRP*, vol. 94, pp. 419-424, 2020. DOI: <https://doi.org/10.1016/j.procir.2020.09.157>
- [40] T. B. Massalski, "Massive transformations," *Material Science and Engineering*, vol. 25, no. 10, pp. 119-125, 1976.
- [41] H. I. Aaronson, "Mechanisms of the massive transformation," *Metallurgical and Materials Transactions A*, vol. 33, no. 8, pp. 2285-2297, Aug. 2002.
- [42] D. M. Wilson, "Metallurgical and mechanical property characterization of additively manufactured 304L stainless steel," M.S. thesis, Metallurgical and Materials Engineering, Colorado School of Mines, Golden, CO, 2019.
- [43] E. Folkhard, G. Rabensteiner, E. Perteneder, H. Schabereiter, and J. Tösch, *Welding Metallurgy of Stainless Steel*. New York: Springer-Verlag Wien, 1988.

- [44] J. C. Lippold and D. J. Kotecki, *Welding Metallurgy and Weldability of Stainless Steels*. New Jersey: John Wiley & Sons, Inc., 2005.
- [45] C. Zhao, K. Fezzaa, R. W. Cunningham, H. Wen, F. De Carlo, L. Chen, A.D. Rollett, and T. Sun, “Real-time monitoring of laser powder bed fusion process using high-speed x-ray imaging and diffraction,” *Scientific Reports*, vol. 7, no. 1, pp. 1-11, Jun. 2017. DOI: <https://doi.org/10.1038/s41598-017-03761-2>